1-1-2012

Studying X-ray burst nucleosynthesis in the laboratory

C. M. Deibel
Louisiana State University

L. Afanasieva
Louisiana State University

M. Albers
Argonne National Laboratory

M. Alcorta
Argonne National Laboratory

S. Almarez-Calderon
Argonne National Laboratory

See next page for additional authors

Recommended Citation

Deibel, C., Afanasieva, L., Albers, M., Alcorta, M., Almarez-Calderon, S., Bedoor, S., Bertone, P., Carnelli, P., Chen, A., Chen, J., Clark, J., Figueira, J., Greene, J., Hoffman, C., Irvine, D., Jiang, C., Kay, B., Lai, J., Lee, H., Lighthall, J., Manwell, S., Marley, S., Nair, C., Palachan-Hazan, T., Pardo, R., Patel, N., Paul, M., Rasco, B., Rehm, K., Rogers, A., Shetty, D., Ugalde, C., & Wuosmaa, A. (2012). Studying X-ray burst nucleosynthesis in the laboratory. *Journal of Physics: Conference Series, 403* (1) https://doi.org/10.1088/1742-6596/403/1/012033

Studying X-ray Burst Nucleosynthesis in the Laboratory

Journal of Physics: Conference Series **403** (2012) 012033 doi:10.1088/1742-6596/403/1/012033

Studying X-ray Burst Nucleosynthesis in the Laboratory

C M Deibel[1,2,3], L Afanasieva[1], M Albers[3], M Alcorta[3], S Almarez-Calderon[3], S Bedoor[4], P F Bertone[3], P Carnelli[5], A A Chen[6], J Chen[3], J A Clark[3], J M Figueira[5], J P Greene[3], C R Hoffman[3], D Irvine[6], C L Jiang[3], B P Kay[3], J Lai[1], H Y Lee[3], J C Lighthall[3,4], S Manwell[6], S T Marley[3,4], C Nair[3], T Palachan-Hazan[3], R C Pardo[3], N Patel[3,7], M Paul[8], B C Rasco[1], K E Rehm[3], A M Rogers[3], D Shetty[4], C Ugalde[3], A Wuosmaa[4], G Zinkann[3]

[1]Department of Physics and Astronomy, Louisiana State University, Baton Rouge, LA 70803 USA
[2]Joint Institute for Nuclear Astrophysics, Michigan State University, East Lansing, MI 48824 USA
[3]Physics Division, Argonne National Laboratory, Argonne, IL 60439 USA
[4]Physics Department Western Michigan University, Kalamazoo, MI 49008 USA
[5]Laboratorio Tandar, Comisión Nacional de Energía Atómica, B1650KNA San Martín, Buenos Aires, Argentina
[6]Department of Physics and Astronomy, McMaster University, Hamilton, ON L8S 4M1, Canada
[7]Department of Physics, Colorado School of Mines, Golden, CO 80401 USA
[8]Racah Institute of Physics, Hebrew University, Jerusalem, Israel

E-mail: deibel@phys.lsu.edu

Abstract. Type I X-ray bursts are the most common explosions in the Galaxy; however, the nucleosynthesis that occurs during the thermonuclear runaway and explosion is poorly understood. In this proceedings we discuss current experimental efforts and techniques that are being used to study X-ray burst nucleosynthesis in the laboratory. Specifically, radioactive ion beam techniques that have recently been developed have allowed the study of some of the most important (α, p) reactions in X-ray bursts for the first time.

1. Introduction

Type I X-ray bursts (XRBs) occur in binary star systems in which hydrogen-rich matter is accreted from a companion, main-sequence star onto the surface of a neutron star at a rate of approximately $10^{-8} - 10^{-10} M_{\odot}$/yr (for an in depth review of X-ray binaries see e.g. [1]). During this accretion phase, while temperatures are approximately 0.1 GK, there is a persistent, thermal X-ray emission. However, as matter is accreted, the pressure and density build up on the neutron star's surface until the extremely temperature-dependent triple-α reaction ignites the burst and thermonuclear runaway occurs. Temperatures of $1 - 2$ GK are reached during XRBs, which typically last for approximately $10 - 100$ s while emitting $10^{39} - 10^{40}$ ergs of energy, increasing

the luminosity of the system by at least an order of magnitude. After the burst, the accretion phase of the system resumes, and the burst cycle begins again, with typical XRB recurrence times on the order of hours to days. Due to the high density of the neutron star, little if any synthesized material escapes the system and most of the nuclei created during the burst become part of the neutron star crust and seeds for subsequent bursts. As a result, these systems are evolving, with each burst affecting those after it. In addition to the seed nuclei from previous bursts, the initial composition before each burst is also affected by the hot-CNO cycle, which burns hydrogen into helium in between bursts.

While most bursts have regular recurrence times and luminosity peaks, there are many observations of irregular bursts. Certain X-ray bursters are observed to undergo so-called "superbursts", which are thought to be due to carbon burning [2] and are typified by larger peak luminosities (several orders of magnitude greater than their typical XRBs) and longer durations and recurrence times. In addition to superbursts there have been several observations of double-peaked bursts [3, 4, 5], and at least one observation of a triple-peaked burst [6]. Several explanations of these multi-peaked bursts have been proposed including stalling of the nuclear burning front [7], as well as a possible nuclear physics solution [8], discussed below.

After the the triple-α reaction triggers the burst, the nucleosynthesis in an XRB is driven up the proton-rich side of stability by the α, p-process and the rapid proton-capture process (rp-process). The α, p-process consists of a series of (α, p) and (p, γ) reactions. Due to the large Coulomb barrier, the (α, p) reaction strongly depends on the temperature of the burst and this process helps to set the time scale of the rise of the burst luminosity curve through the effects of so-called waiting points. There have been four potential α, p-process waiting points identified: ^{22}Mg, ^{26}Si, ^{30}S, and ^{34}Ar [9]. These (Z-N)/2 = 1 nuclei have low $Q_{p,\gamma}$ values and thus come into a (p, γ)-(γ, p) equilibrium with their Z+1 counterparts and must await β^+ decay, stalling the nucleosynthetic flow. As these nuclei have half-lives on the order of seconds this delay can be significant on XRB time scales. However, if a competing reaction, such as the (α, p) reaction, is fast enough, breakout from the waiting point occurs and nucleosynthesis continues up the chart of nuclides. Therefore, it is important to understand the different processes occurring at a waiting-point nucleus in a self consistent way. Additionally, these waiting points have been suggested as a possible mechanism for the observed double-peaked structure of some XRB light curves, as the stalling of the nucleosynthetic flow may cause a decrease in the energy generated by the burst and thus a dip in the luminosity profile [8].

The rp-process is a series of (p, γ) reactions and β decays that extend the nucleosynthesis up to higher masses. The endpoint of the rp-process in XRBs is thought to be in the SnSbTe region; however, this remains uncertain as on one hand there is evidence for a weak SnSbTe cycle that would move the rp-process path closer to stability [10], while on the other hand some models show leakage out of the SbSnTe cycle to higher mass nuclei [11]. Higher-mass waiting points in the rp-process, which occur at nuclei with long β-decay half-lives and small proton-capture Q values, govern the shape of the decay of the light curve.

In order to understand XRB nucleosynthesis fully, three types of nuclear data are required: well-known masses of the nuclei involved, their β-decay rates, and the rates of reactions that occur in XRBs. Recently, there have been multiple advances in each of these areas (see e.g. [12] for recent mass measurements and [13] for β-decay lifetime measurements). Due to the proton-rich nuclei that are involved in XRB nucleosynthesis, many of the thousands of reactions and processes that occur in these explosive environments are not directly accessible in the laboratory. As a result, theoretical values are used for the nuclear input data in stellar models of XRBs where experimental data does not exist. However, the uncertainty associated with these theoretical values can be very high and those predictions do not always agree with experimental data when they become available.

Some of the unstable nuclei of interest are close enough to stability that they can be accessed

using stable beams and targets that are easily produced [14]. However, many of these reactions and nuclei are too far from stability to be studied using stable beams. With the advent of radioactive ion beam (RIB) facilities, some of the processes involving these nuclei can now be studied for the first time. For reaction rates specifically one would ideally like to study them directly [15]; however, even with these new advances in RIB technology, direct measurements are still extremely difficult and often impossible. Therefore, indirect methods with both stable and radioactive ion beams must be used. This proceedings article reviews experimental advances in the determination of (α, p) reaction rates that are important in XRBs, which have just recently been made possible by radioactive ion beam facilities that are now available.

2. Experiment

The (α, p) reactions on all four waiting-point nuclei (^{22}Mg, ^{26}Si, ^{30}S, and ^{34}Ar) have been studied via the time-inverse (p, α) reactions measured in inverse kinematics with RIBs. These RIBs were produced at Argonne National Laboratory using the "in-flight" facility at the Argonne Tandem Linac Accelerator System (ATLAS). Stable beams of ^{24}Mg, ^{28}Si, ^{32}S, and ^{36}Ar were accelerated to energies of approximately 315 - 325 MeV and impinged upon a LN_2-cooled gas target filled with 1.4 atm of D_2 gas. Radioactive ion beams of ^{25}Al, ^{29}P, ^{33}Cl, and ^{37}K with energies of 253, 280, 250, and 275 MeV, respectively, were produced via (d, n) reactions with the stable beams. The radioactive ions of interest were then refocused, rebunched and separated by an analyzing magnet from the stable component of the beam. Typically the low energy tail of the unreacted stable beam is also selected by the analyzing magnet resulting in an unfavorable ratio of approximately 1:1000 radioactive ions/s to stable ions/s. As these two components of the resulting "cocktail" beam are separated in time of flight, a radio-frequency (RF) sweeper is used to eliminate much of the stable beam contamination improving the radioactive to stable beam ratio to better than 1:1. The intensities of the RIBs ranged from $1 - 5 \times 10^4$ ions/s depending on the RIB species.

Changing the energy of the RIB to scan through the energy region of interest for the reaction by changing the energy of the primary, stable beam would be prohibitively time consuming given the difficulty of producing and tuning RIBs. Therefore, in order to change beam energies Au degrader foils of different thicknesses were used. The thicknesses of the Au foils were chosen such that the energy loss of the beam in the target would be approximately the same as the energy loss in the foils (approximately 10 MeV in the case of a 250 MeV ^{33}Cl beam).

Once the RIB has been produced it is delivered to the experimental area where it impinges on a CH_2 target of approximately 650 μg/cm^2. The α particles produced from the (p, α) reactions are detected in an annular double-sided Si detector (DSSD) that is segmented in θ_{lab} (see Fig. 1). The DSSD was placed such that lab angles of $6^\circ - 19^\circ$ were covered for the $p(^{25}\mathrm{Al},^{22}\mathrm{Mg})\alpha$ and $p(^{29}\mathrm{P},^{26}\mathrm{Si})\alpha$ reactions and $8^\circ - 24^\circ$ were covered in the $p(^{33}\mathrm{Cl},^{30}\mathrm{S})\alpha$ and $p(^{37}\mathrm{K},^{34}\mathrm{Ar})\alpha$ reaction studies.

The heavy-ion recoils along with the unreacted beam (from both the RIB and the stable contaminant) were momentum-analyzed by an Enge split-pole spectrograph. The reaction products of interest were separated from other heavy ions by the spectrograph, which was run in gas-filled mode, filled with approximately 15 Torr of N_2 gas in the case of the highest beam energies. The gas-filled mode was used to collapse the charge state distribution of the heavy-ion recoils into a single charge state [16] to maximize detection efficiency at the focal plane, which is crucial in these types of low-statistics experiments, as well as to avoid position overlap of the reaction products of interest and unreacted beam in various charge states. Once the heavy recoils passed through the spectrograph, they were detected at the focal plane by a gas-filled parallel grid avalanche counter (PGAC) and an ionization chamber. These detectors give position and energy loss of the ions, as well as time-of-flight of the ions relative to the RF of the beam, allowing particle identification. By detecting the heavy-ion recoils in coincidence

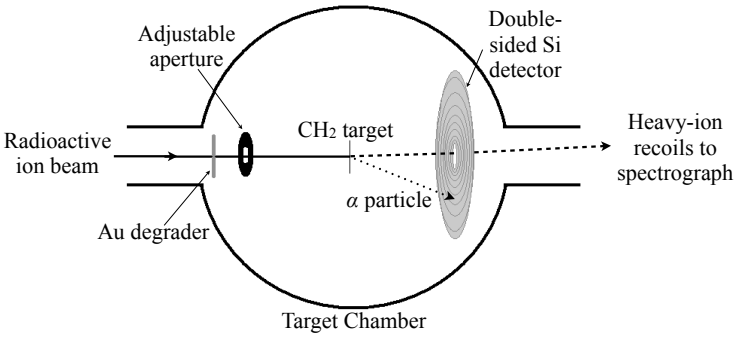

Figure 1. A schematic of the experimental setup.

with the α particles, correcting for efficiencies, and normalizing to the incident beam and target thickness, the cross section of the reaction of interest can be determined.

3. Analysis and Results

The α particles were detected by the DSSD in coincidence with the heavy-ion recoils as discussed above to determine the α-particle yield for the reaction. Background was partially eliminated through particle identification cuts on the time-of-flight and focal plane position (or equivalently magnetic rigidity) of the heavy recoils. Additional background was subtracted by determining the random background rate outside of the coincidence timing cut. Once the α-particle yield was determined it was corrected for various efficiencies and normalized to the incident beam and target areal density.

Unfortunately, as the magnetic rigidity of the high-energy heavy recoils associated with the low-energy α branch is the same as the magnetic rigidity of the unreacted beam, those recoils were blocked from entering the detector to avoid overwhelmingly high count rates and only the high-energy α branch of the reaction could be measured. The efficiency factor for detecting only the high-energy α branch is approximately 0.67 (e.g. for $p(^{33}\mathrm{Cl},^{30}\mathrm{S})\alpha$) as determined via Monte Carlo simulations. The geometrical efficiencies of the DSSD and spectrograph were 0.82 and 0.38, respectively, also determined via Monte Carlo simulations.

Normalization to the incident beam and target was done in several ways. For the $p(^{33}\mathrm{Cl},^{30}\mathrm{S})\alpha$ measurement, the ratio of Rutherford scattering off the carbon component of the CH_2 target at 2.5°, measured in the spectrograph, to the proton scattering at 8°, measured in the inner ring of the DSSD, was determined in a separate measurement during the experiment. The proton scattering was then monitored throughout the (p,α) experiment and using the ratio defined above with the calculated Rutherford cross section, normalization to the incident beam and target was achieved. In addition, for all the (p,α) measurements, the beam intensity and composition was checked every few hours by measuring it directly in the spectrograph after attenuation. Both methods of normalization agreed to within error. An additional Si surface barrier detector was used as an added check in both the $p(^{25}\mathrm{Al},^{22}\mathrm{Mg})\alpha$ and $p(^{37}\mathrm{K},^{34}\mathrm{Ar})\alpha$ measurements to monitor the beam intensity and target thickness.

Once the α-particle yield was corrected for efficiencies and normalized, the cross section could then be compared with theoretical calculations, such as those from the NON-SMOKER code [17, 18, 19] (see e.g. Fig. 2 for the case of $p(^{33}\mathrm{Cl},^{30}\mathrm{S})\alpha$ [20]).

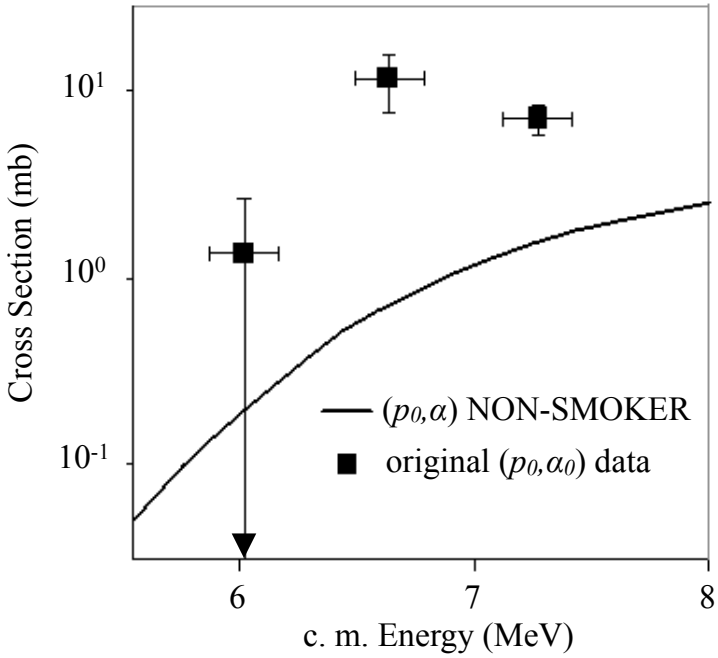

Figure 2. Cross section as a function of c.m. energy for the ^{33}Cl$(p_0, \alpha_0)^{30}$S data (squares) and the NON-SMOKER calculations [17, 18, 19] for the ^{33}Cl$(p_0, \alpha)^{30}$S cross section (solid line). The experimental data only include ground state to ground state transitions, while the NON-SMOKER calculations include transitions to excited states. The vertical error bars indicate the uncertainties in the cross sections and the horizontal error bars indicate the energy spread of the beam in the target. Reproduced from [20].

4. Conclusions

It can clearly be seen from Fig. 2 that the experimental data do not agree with theoretical calculations from NON-SMOKER and are up to a factor of four higher than the theoretical cross sections. Indeed the disagreement may be worse than what is shown in Fig. 2 since the measured cross sections are lower limits as they do not contain any possible contribution from transitions to excited states in the final nucleus. Furthermore, for the other reactions measured, preliminary results also show disagreement with theoretical calculations, although not always in the same direction. For example, the measurement of the $p(^{37}\mathrm{K},^{34}\mathrm{Ar})\alpha$ reaction gives cross sections that are significantly lower than NON-SMOKER predictions [21]. Of course, given that the cross section for the forward ^{34}Ar$(\alpha, p)^{37}$K reaction is only a lower limit, as it does not contain any transitions to excited states in the final ^{37}K nucleus, it is possible that the total cross section for the (α, p) reaction could agree with the theoretical predictions in this case.

This disagreement between experimental measurements and NON-SMOKER calculations is not altogether surprising as these calculations are based on Hauser-Fesbach theory that assumes high level densities, which may not be valid in this mass regime. In this intermediate mass region the level densities for even-even nuclei are expected to be low in the astrophysically relevant energy regime and thus the reaction rate may be dominated by a few isolated resonances. It should be noted that the energies measured for each reaction described here are above this energy region of interest. Given the rapidly decreasing cross section with energy and the low-intensity RIBs available, it was not feasible to measure the cross sections in the region of interest (e.g. $\mathrm{E}_{c.m.} = 3.5 - 4.4$ MeV for $p(^{33}\mathrm{Cl},^{30}\mathrm{S})\alpha$) during these experiments. However, the results of these

measurements underscore the need to experimentally determine the rates of the reactions of interest in XRB nucleosynthesis, as the theoretical calculations (e.g. NON-SMOKER) currently used in stellar models do not accurately reproduce measured data.

Although the measurements presented here are above the energy range of interest for XRB nucleosynthesis, the discrepancies between the measured and theoretical cross sections will have implications for stellar models of XRBs if they persist at lower energies. For example, in the case of ^{30}S$(\alpha, p)^{33}$Cl, which clearly shows higher cross sections than the theoretical calculations in the energy regime measured, a higher reaction rate would lead to break out of the ^{30}S waiting point. This would imply that the ^{30}S waiting point is not responsible for the double-peaked structure of certain observed luminosity profiles, as the nucleosynthesis flows more readily through ^{30}S. The additional effects of the measured cross sections of the (α, p) reactions on ^{30}S and other waiting-point nuclei on XRB nucleosynthesis will be addressed in a future publication.

In addition to accurate reaction rates, measurements of nuclear masses and β decay rates also continue to be needed and experimental advances on all three of these fronts are progressing as more radioactive ion facilities become available. Stable beam data also continue to provide new insight into XRB nucleosynthesis [14] and are necessary even as RIB capabilities increase. In order to fully understand these astrophysical environments accurate nuclear data is needed as input for stellar models. While theoretical determinations of these parameters fill the gaps where no data exist, until those models can reliably reproduce experimental data, measurements are needed to ensure an accurate description of these stellar events.

Acknowledgments

The authors would like to thank the ATLAS operators and staff for their assistance during these experimental studies. We would also like to acknowledge funding from NSF JINA grant No. PHY0822648 and U.S. DOE contract No. DE-AC02-06CH11357. We would finally like to thank T. Rauscher for helpful discussions regarding NON-SMOKER code calculations.

References

[1] Schatz H and Rehm K E 2006 *Nucl. Phys.* **A777** 601
[2] Cooper R L, Steiner A W and Brown E F 2009 *Astrophys. J.* **702** 660
[3] Sztajno M, van Paradijs J, Lewin W H G, Trümper J, Stollman G, Pietsch W and van der Klis M 1985 *Astrophys. J.* **299** 487
[4] Penninx W, van Paradijs J and Lewin W H G 1987 *Astrophys. J. Lett.* **321** 67
[5] Kuulkers E, Homan J, van der Klis M, Lewin W H G and Méndez M 2002 *Astron. Astrophys.* **382** 947
[6] Zhang G, Mendez M, Altamirano D, Belloni T M and Homan J 2009 *Mon. Not. R. Astron. Soc.* **389** 368
[7] Bhattacharyya S and Strohmayer T E 2006 *Astrophys. J.* **641** L53
[8] Fisker J L, Thielemann F K and Wiescher M 2004 *Astrophys. J. Lett.* **608** 61
[9] Fisker J L, Schatz H and Thielemann F K 2008 *Astrophys. J. SS.* **174** 261
[10] Elomaa V V, Voobjev G K, Kankainen A, Batist L, Eliseev S, Eronen T, Hakala J, Jokinen A, Moore I D, Novikov Y N, Penttilä H, Popov A, Rahaman S, Rissanen J, Saastamoninen A, Schatz H, Seliverstov D M, Weber C and Äystö J 2009 *Phys. Rev. Lett.* **102** 252501
[11] José J, Moreno F, Parikh A and Iliadis C 2010 *Astrophys. J. Supp. Ser.* **189** 204
[12] Tu X L *et al.* 2011 *Phys. Rev. Lett.* **106** 112501
[13] Nishimura S *et al.* 2011 *Phys. Rev. Lett.* **106** 052502
[14] Setoodehnia K *et al.* 2010 *Phys. Rev. C* **82** 022801(R)
[15] Chen A A *et al.* 2005 *Nucl. Phys.* **A752** 510
[16] Paul M *et al.* 1989 *Nucl. Inst. Meth. Phys. Res.* **A277** 418
[17] Rauscher T and Thielemann F K 2000 *Atomic Data and Nuclear Data Tables* **75** 1
[18] Rauscher T and Thielemann F K 2001 *At. Data Nucl. Data Tables* **79** 47
[19] Non-smoker code, http://nucastro.org/nonsmoker.html
[20] Deibel C M, Rehm K E, Clark J A, Figueira J M, Jiang C L, Kay B P, Lee H Y, Marley S T, Pardo R C, Patel N *et al.* 2009 ATLAS PAC proposal 1279
[21] Deibel C M *et al.* in preparation